Position Control of an Electro-Pneumatic Clutch Using Takagi-Sugeno Techniques

Robert Prabel[*] and Harald Aschemann[*]
[*]*Chair of Mechatronics, University of Rostock, Rostock, Germany*

Summary. The paper presents a nonlinear control design for the position of an electro-pneumatic clutch that is based on a nonlinear mathematical model. Regarding the lower and upper bounds of the nonlinear terms involved, a fuzzy Takagi-Sugeno (TS) description with four corner models in a polytopic framework can be used for the control design. The feedback control gains are calculated for each corner model, and the overall adaptive feedback gain vector results from a norm-optimal combination of the individual feedback actions of these corner models. For an improvement of the tracking behaviour of the clutch, the control structure is extended by a dynamic feedforward control as well as an observer-based disturbance compensation. Here, a lumped disturbance force is estimated by a gain-scheduled sliding mode observer. The benefits of the proposed control structure are demonstrated by experimental results from a dedicated test rig.

1. Introduction and Motivation

Vehicles with an internal combustion engine as the prime mover are typically equipped with a clutch – either manually or automatically actuated –, which is especially needed during start-up phases. To increase the comfort and to allow for automated transmissions, feedback-controlled clutch systems as central components are required. In the literature, different models for the calculation of the transmitted torque can be found, e.g. [7], [8] and [11]. Typically, algebraic equations for the transmitted torque are of the form

$$T_{cl} = n_{cl} R_\mu F_N \,, \tag{1}$$

where n_{cl} is the number of friction discs. The equivalent friction radius R_μ mainly depends on the temperature of the friction discs as well as the relative angular velocity between the motor and the gear box input shaft. F_N represents the normal force acting on friction disc, which can be adjusted by an automated clutch actuator. In heavy truck applications with up to 16 gears, a electro-pneumatic solution is typically installed, and this actuator is position-controlled. The relationship between the position of the clutch actuator z and the resulting normal force F_N is depicted in Fig. 1b, where z_{zu} represents the position of the completely closed clutch. Here, the clutch can transmit the maximum torque of the internal

(a) Test rig for the electro-pneumatic clutch.

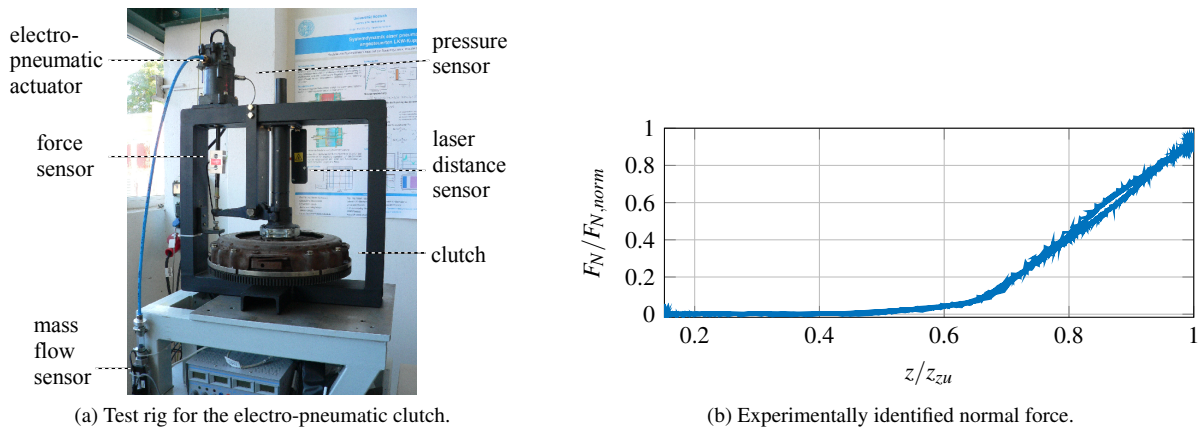(b) Experimentally identified normal force.

Figure 1: Test rig at the Chair of Mechatronics, University of Rostock.

combustion engine. Usually, gain-scheduled PD- or PI-controllers extended by suitable feedforward control actions are employed in industrial solutions. However, more accurate nonlinear control concepts can be found in [1], [6] and [9], where the nonlinearities in the pneumatic subsystem as well as hysteresis in the nonlinear clutch force characteristic are properly addressed. In this paper, a TS control approach is presented and applied to a clutch test rig, which is available at the Chair of Mechatronics, University of Rostock, see Fig. 1a. Control designs based on TS techniques have been successfully applied to several nonlinear problems, see [4] and [5]. The outline of this paper is as follows: Control-oriented models for the mechanical and pneumatic subsystem are derived in Sect. 2. Next, based one a quasi-linear state-space representation, a TS control approach for the position of the clutch is derived in Sect. 3. Furthermore, a sliding mode state observer is introduced, see Sect. 4. Besides, the overall control structure is validated in experiments, see Sect. 5. Finally, the paper concludes with a short summary of this contribution.

2. Modelling of the Clutch Actuator

Pulse-width-modulated on/off valves are used to provide the inlet and outlet air mass flows for the pneumatic chamber of the actuator. Thereby, the internal pressure in the pneumatic cylinder changes, and finally drives the piston. The nonlinear

model of the electro-pneumatic clutch can be divided into a mechanical and a pneumatic subsystem. Fig. 2a shows the mechatronic model of the system. The considered operation range is limited by positive values $0 < z < z_{zu} \leq l_{max}$. Due to the wear of the friction pad during operation, the position z_{zu} of the fully closed clutch increases slowly.
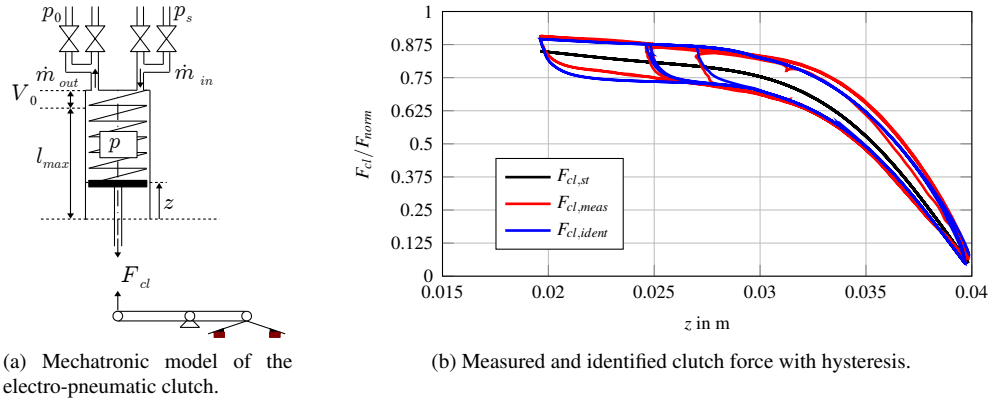

(a) Mechatronic model of the electro-pneumatic clutch.

(b) Measured and identified clutch force with hysteresis.

Figure 2: Structure of an electro-pneumatic clutch (a) and normalised nonlinear characteristics of the clutch force (b).

Mechanical Subsystem

The acceleration of the piston rod results directly from Newton's second law

$$\ddot{z} = \frac{1}{m}[F_{cl} - A_k(p - p_0) - c_{sp}(z_{sp} + z) - F_U],\qquad(2)$$

with m as the reduced mass of all the moving components of the pneumatic clutch, A_k as the piston surface and p_0 as the ambient pressure. Furthermore, a pre-load force $z_{sp}c_{sp}$ of a spring with the stiffness c_{sp}, the nonlinear clutch force F_{cl} and a lumped disturbance force F_U are introduced. Moreover, the nonlinear clutch force

$$F_{cl} = F_{cl,st} + F_{cl,hys}\qquad(3)$$

can be divided in a static part $F_{cl,st}$ – representing the medium curve – and a hysteresis part $F_{cl,hys}$. A detailed modelling with a sixth-degree polynomial ansatz function for the medium clutch force is presented in [2], which is also employed in this paper. The hysteresis part of the clutch force describing the deviation from the medium curve $F_{cl,st}(z)$ is modelled by the generalised Bouc-Wen model $F_{cl,hys} = F_{cl,hys}(z, \xi)$. Detailed information regarding the implemented Bouc-Wen model as well as its parametrisation is provided in [1]. The modelling results are depicted in Fig. 2b.

Pneumatic Subsystem

Pressurised air is used for the actuation of the clutch. A control-oriented model for the pneumatic subsystem based on a mass flow balance in combination with a polytropic change of thermodynamic state for the compressed air in the pneumatic chamber can be found in [1] and [2]. The resulting differential equation for the internal pressure is given by

$$\dot{p} = \frac{nR_L T \dot{m}}{V(z)} + \frac{pnA_k\dot{z}}{V(z)},\qquad(4)$$

with the actual volume of the cylinder chamber $V(z) = V_0 + A_k(l_{max} - z)$. The parameters in (4) are the gas constant of air R_L, the polytropic exponent n, and the resulting sum $\dot{m}$ of the inlet and outlet mass flows. For a simplification of the mechatronic model, the internal temperature T is parametrised with the constant temperature T_{amb} of the ambiance. To simplify the control design for the inner loop, the term $u(t) = R_L \cdot T_{amb} \cdot \dot{m}(t)$ is introduced as control input.

Valve Actuation

Pulse-width-modulated on/off valves are used to control the inlet and outlet mass flow $\dot{m}$. Compared to proportional valves, on/off valves are much cheaper and more energy efficient. Instead of using the PWM signal and mathematical description for the mass flow, an experimentally identification of the mass flow characteristic has been carried out, see Fig. 3. An corresponding approximative inverse can be derived numerically with high accuracy. A pre-multiplication with this inverse valve characteristic practically linearises the nonlinear valve characteristic.
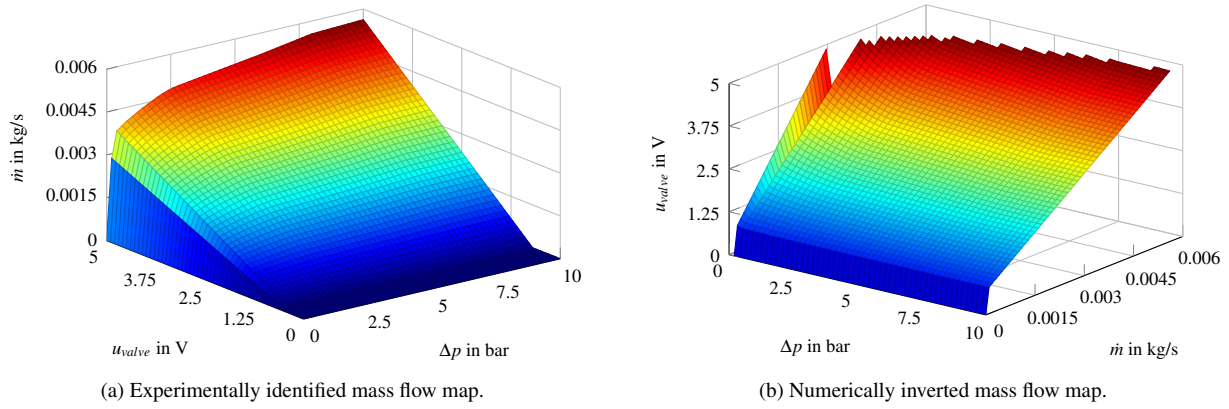
(a) Experimentally identified mass flow map.

(b) Numerically inverted mass flow map.

Figure 3: Identified (a) and inverted (b) mass flow map of one selected valve.

3. TS Control Design for the Position of the Clutch

As a basis of the feedback control design, the nonlinear mathematical model – with the state vector $\underline{x} = [z \; \dot{z} \; p]^T$ as well as the control input $u = R_L T \dot{m}$ – is rewritten as a quasi-linear state-space representation

$$\dot{\underline{x}} = \underline{A}(z,\dot{z}) \, \underline{x} + \underline{b}(z) \, u + \underline{e} \, F_{Dis}$$

$$= \begin{bmatrix} 0 & 1 & 0 \\ \dfrac{-c_{sp}}{m} & \dfrac{-b}{m} & \dfrac{-A_k}{m} \\ 0 & 0 & nA_k f_1(z,\dot{z}) \end{bmatrix} \begin{bmatrix} z \\ \dot{z} \\ p \end{bmatrix} + \begin{bmatrix} 0 \\ 0 \\ n f_2(z) \end{bmatrix} u + \begin{bmatrix} 0 \\ \dfrac{-1}{m} \\ 0 \end{bmatrix} \underbrace{[c_{sp} z_{sp} - A_k p_0 - F_{cl} + F_U]}_{F_{Dis}} , \tag{5}$$

where the nonlinear terms

$$f_1(z,\dot{z}) = \frac{\dot{z}}{V_0 + A_k \, (l_{max} - z)} , \tag{6}$$

$$f_2(z) = \frac{1}{V_0 + A_k \, (l_{max} - z)} \tag{7}$$

depend on the clutch position as well on the velocity. Note that this quasi-linear representation is still exact and does not involve any approximation. Considering the lower and upper bounds of the nonlinear terms, the constant system matrices of the corner models

$$\underline{A}_1 = \underline{A}(\max f_1, \max f_2), \; \underline{A}_2 = \underline{A}(\max f_1, \min f_2), \; \underline{A}_3 = \underline{A}(\min f_1, \max f_2) \text{ and } \underline{A}_4 = \underline{A}(\min f_1, \min f_2) \tag{8}$$

as well as the constant input vectors

$$\underline{b}_1 = \underline{b}(\max f_1, \max f_2), \; \underline{b}_2 = \underline{b}(\max f_1, \min f_2), \; \underline{b}_3 = \underline{b}(\min f_1, \max f_2) \text{ and } \underline{b}_4 = \underline{b}(\min f_1, \min f_2) \tag{9}$$

can be introduced. Given the normalizing conditions $w_{i,1} + w_{i,2} = 1$, the ansatz $w_{i,j}$ for the weighting functions with $0 \leq w_{i,j} \leq 1$, $i \in \{1,2\}$ and $j \in \{1,2\}$, is as follows

$$f_i(z,\dot{z}) = w_{i,1} \max f_i + w_{i,2} \min f_i . \tag{10}$$

The solution leads to the following expressions

$$w_{i,1}(z,\dot{z}) = \frac{f_i(z,\dot{z}) - \min f_i}{\max f_i - \min f_i} ,$$

$$w_{i,2}(z,\dot{z}) = \frac{\max f_i - f_i(z,\dot{z})}{\max f_i - \min f_i} , \tag{11}$$

which allow for an exact interpolation of the corner systems with the given bounds. After some formula manipulations, the membership functions of the four corner models result in

$$h_1(z,\dot{z}) = w_{11}(z,\dot{z}) \, w_{21}(z) , \; h_2(z,\dot{z}) = w_{11}(z,\dot{z}) \, w_{22}(z) , \; h_3(z,\dot{z}) = w_{12}(z,\dot{z}) \, w_{21}(z) \text{ and } h_4(z,\dot{z}) = w_{12}(z,\dot{z}) \, w_{22}(z). \tag{12}$$

Now, the exact quasi-linear state representation (5) can be rewritten as

$$\dot{\underline{x}} = \sum_{l=1}^{4} h_l(z,\dot{z}) \left[\underline{A}_l(z,\dot{z}) \, \underline{x} + \underline{b}_l(z) \, u \right] + \underline{e} \, F_{Dis} . \tag{13}$$

(a) Membership function $h_1(z,\dot{z})$.

(b) Membership function $h_2(z,\dot{z})$.

(c) Membership function $h_3(z,\dot{z})$.
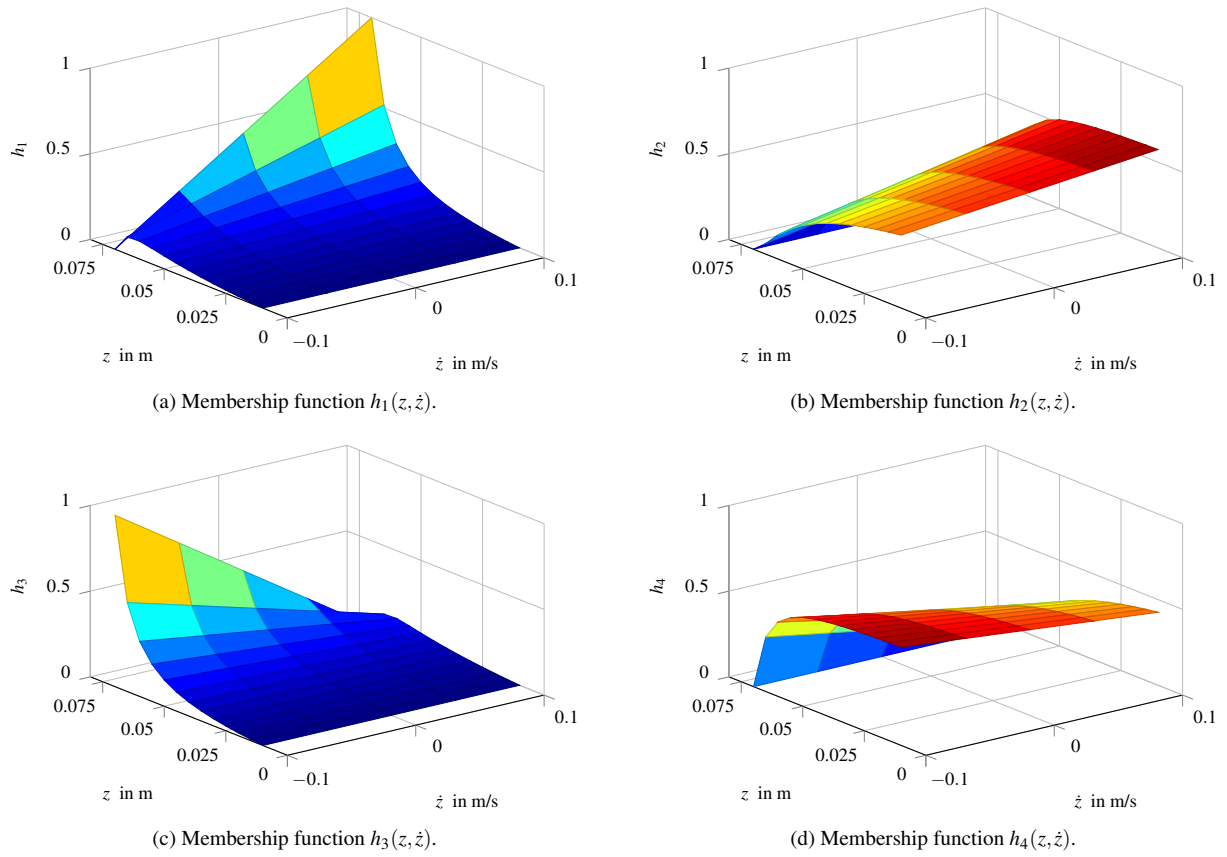
(d) Membership function $h_4(z,\dot{z})$.

Figure 4: Membership functions of the corner models of the polytope.

State-Feedback Design Using Eigenvalue Placement

The state feedback $\underline{k}_l^T$, $l \in \{1,2,3,4\}$, is designed by an eigenvalue placement for each corner system. Therefore, the gain vector $\underline{k}_l^T$ is calculated by a comparison of the desired characteristic polynomial of the closed-loop system

$$p_{c,d}(s) = (s - s_{c1})(s - s_{c2})(s - s_{c3}) , \quad \text{with } s_{ci} < 0, \ i \in \{1,2,3\}, \tag{14}$$

specifying three eigenvalues s_{ci} for the characteristic equation for each corner model

$$p_c(s) = \det\left(s\underline{I}_3 - \underline{A}_l + \underline{b}_l \underline{k}_l^T\right) = \det\left(s\underline{I}_3 - \underline{A}_{c,l}\right), \ l \in \{1,2,3,4\} , \tag{15}$$

where $\underline{I}_3$ is the 3x3 identity matrix and $\underline{A}_{c,l}$ the closed-loop system matrix in each corner l of the polytope. Typically, a parallel-distributed compensator (PDC), see [10] for details, is employed for the feedback control of TS state-space models

$$u_{FB}(z,\dot{z}) = -\sum_{l=1}^{4} h_l(z,\dot{z}) \underline{k}_l^T \underline{x} , \tag{16}$$
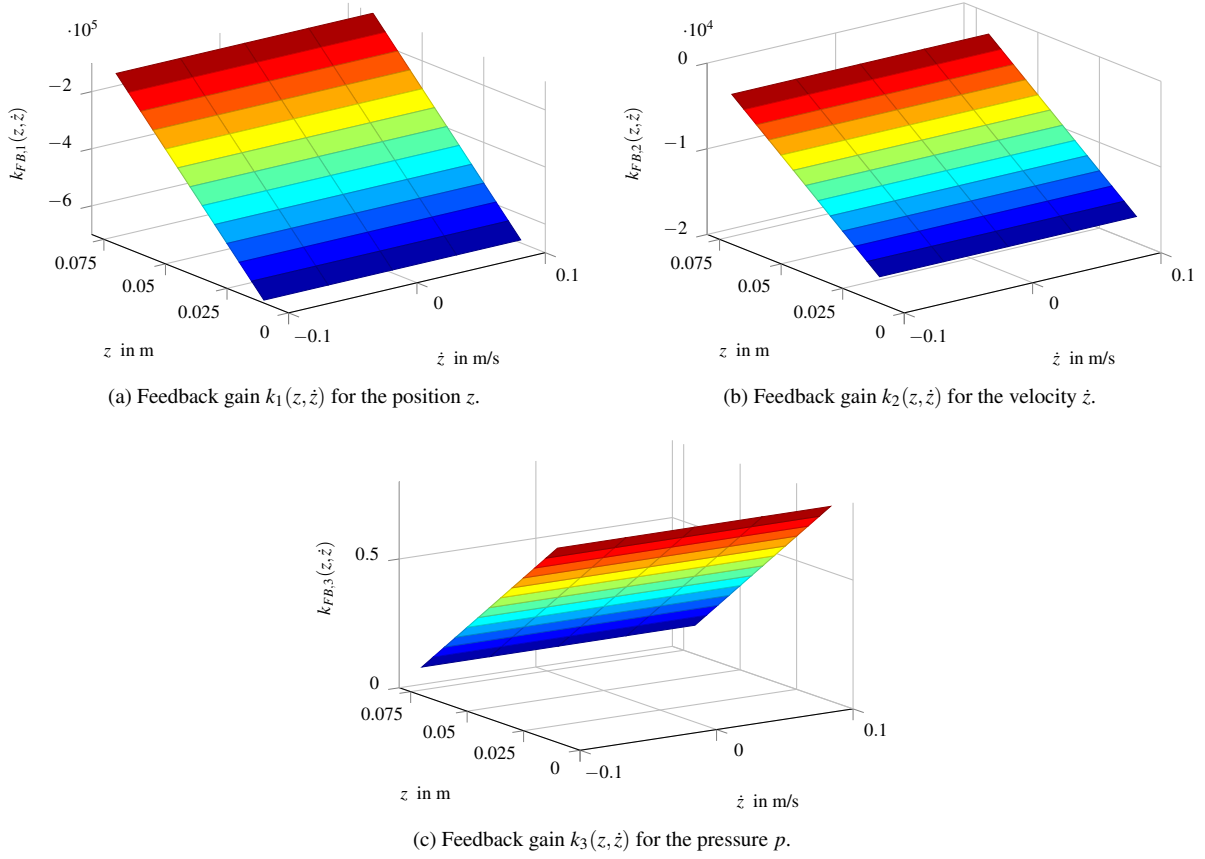
which requires the use of linear matrix inequalities (LMIs) for the stability proof. Here, an alternative approach is proposed using the following design condition

$$\underbrace{\sum_{l=1}^{4} [h_l(z,\dot{z}) \underline{b}_l]}_{\underline{b}(z)} \underline{k}^T(z,\dot{z}) = \underline{b}(z) \underline{k}^T(z,\dot{z}) = \sum_{l=1}^{4} [h_l(z,\dot{z}) \underline{b}_l \underline{k}_l^T]. \tag{17}$$

This condition cannot fulfilled exactly but the equation error can be minimized in a least-squares sense. This leads to a norm-optimal solution based on the pseudo-inverse of $\underline{b}(z)$ according to

$$\underline{k}^T(z,\dot{z}) = (\underline{b}^T(z) \underline{b}(z))^{-1} \underline{b}^T(z) \left[h_1(z,\dot{z}) \underline{b}_1 \underline{k}_1^T + h_2(z,\dot{z}) \underline{b}_2 \underline{k}_2^T + h_3(z,\dot{z}) \underline{b}_3 \underline{k}_3^T + h_4(z,\dot{z}) \underline{b}_4 \underline{k}_4^T \right] , \tag{18}$$

which interpolates between the constant control gain vectors $\underline{k}_l^T$ of the corner models. The overall state-dependent feedback gains are shown in Fig. 5.

(a) Feedback gain $k_1(z,\dot{z})$ for the position z.

(b) Feedback gain $k_2(z,\dot{z})$ for the velocity $\dot{z}$.

(c) Feedback gain $k_3(z,\dot{z})$ for the pressure p.

Figure 5: State-dependent overall feedback gains $\underline{k}^T(z,\dot{z})$.

The controlled system can be stated as

$$\dot{\underline{x}} = \underbrace{\left(\underline{A}(z,\dot{z}) - \underline{b}(z)\,\underline{k}^T(z,\dot{z})\right)}_{\underline{A}_c(z,\dot{z})} \underline{x} + \underline{e}\,F_{Dis}, \text{ with}$$

$$\underline{A}(z,\dot{z}) = \sum_{l=1}^{4} h_l(z,\dot{z})\underline{A}_l\,,$$

$$\underline{b}(z) = \sum_{l=1}^{4} h_l(z,\dot{z})\underline{b}_l\,. \tag{19}$$

Here, the system matrix of the closed-loop system $\underline{A}_c(z,\dot{z})$ turns out to be constant

$$\underline{A}_c(z,\dot{z}) = \underline{A}(z,\dot{z}) - \underline{b}(z)\,\underline{k}^T(z,\dot{z}) = \begin{bmatrix} 0 & 1 & 0 \\ \dfrac{-c_{sp}}{m} & \dfrac{-b}{m} & \dfrac{-A_k}{m} \\ a_{c,3,1} & a_{c,3,2} & a_{c,3,3} \end{bmatrix} = const. \tag{20}$$

The constant matrix elements read as follows

$$a_{c,3,1} = \frac{1}{A_k}\left(-m\,s_{c1}\,s_{c2}\,s_{c3} + c_{sp}\,(s_{c1}+s_{c2}+s_{c3}) + \frac{b\,c_{sp}}{m}\right),$$

$$a_{c,3,2} = \frac{m}{A_k}\,(s_{c1}s_{c2}+s_{c1}s_{c3}+s_{c2}s_{c3}) + \frac{b}{A_k}\,(s_{c1}+s_{c2}+s_{c3}) + \frac{b^2}{A_k\,m} - \frac{c_{sp}}{A_k},$$

$$a_{c,3,3} = s_{c1}+s_{c2}+s_{c3} + \frac{b}{m}\,. \tag{21}$$

Given the constant system matrix, the closed-loop stability is guaranteed by the specified eigenvalues in the left s-half-plane.

Feedforward Control Design
Considering the position of the clutch as controlled state variable

$$y = z = [1\ 0\ 0]\underline{x} = \underline{c}^T\,\underline{x}\,, \tag{22}$$

the command transfer function results in

$$\frac{Y(s)}{U_{FF}(s)} = \underline{c}^T [s\underline{I} - \underbrace{(\underline{A}(z,\dot{z}) - \underline{b}(z)\,\underline{k}^T(z,\dot{z}))}_{=\underline{A}_c}]^{-1}\underline{b}(z) = \frac{b_0}{N(s)}. \tag{23}$$

Obviously, the numerator of the command transfer function does not contain any zero. The main idea of the feedforward control design is the modification of the numerator of the control transfer function by introducing a polynomial ansatz for the feedforward control action in the Laplace domain according to

$$U_{FF}(s) = \left[k_{V0} + k_{V1}\cdot s + k_{V2}\cdot s^2 + k_{V3}\cdot s^3\right] Y_d(s). \tag{24}$$

A comparison of the coefficients in the numerator as well as the denominator polynomials leads to $a_i = b_0 \cdot k_{Vi}, i = \{0,\ldots,n=3\}$. The corresponding position-dependent feedforward gains results in

$$k_{V0}(z_d) = \frac{s_{c1}\,s_{c2}\,s_{c3}\,m\,V(z_d)}{A_k\,n},$$

$$k_{V1}(z_d) = -\frac{(s_{c1}\,s_{c2} + s_{c1}\,s_{c3} + s_{c2}\,s_{c3})\,m\,V(z_d)}{A_k\,n},$$

$$k_{V2}(z_d) = \frac{(s_{c1} + s_{c2} + s_{c3})\,m\,V(z_d)}{A_k\,n},$$

$$k_{V3}(z_d) = -\frac{m\,V(z_d)}{A_k\,n}. \tag{25}$$

These feedforward gains are evaluated with desired values z_d for the clutch position. For its implementation, the desired trajectory $y_d(t) = z_d(t)$ as well as the first three time derivatives are available from a state variable filter.

Dynamic Disturbance Compensation

To improve the tracking behaviour a disturbance compensation is essential. According to (5), the overall disturbance force $F_{Dis} = c_{sp}\,z_{sp} - A_k\,p_0 - F_{cl} + F_U$ depends on the spring pre-load $c_{sp}\,z_{sp}$, the ambient pressure force $A_k\,p_0$, the clutch force F_{cl}, and a unknown force F_U that takes into account parameter uncertainty as well as unmodelled nonlinear friction. This resulting disturbance force F_{Dis} has to be compensated as good as possible to achieve an accurate tracking behaviour. Therefore, a dynamic disturbance compensation is employed. The corresponding disturbance transfer function from the disturbance input to the controlled output becomes

$$G_e(s) = \frac{Y(s)}{F_{Dis}(s)} = \underline{c}^T [s\underline{I} - \underbrace{(\underline{A}(z,\dot{z}) - \underline{b}(z)\,\underline{k}^T(z,\dot{z}))}_{=\underline{A}_c}]^{-1}\underline{e}. \tag{26}$$

For an ideal disturbance compensation, the condition

$$Y(s) = G_b(s)\cdot U_{DC}(s) + G_e(s)\cdot F_{Dis}(s) \overset{!}{=} 0 \tag{27}$$

has to be fulfilled. For this purpose, an ansatz function for the disturbance compensation is made according to

$$U_{DC}(s) = G_{DC}(s)\cdot F_{Dis}(s) = \left[k_{DC0} + k_{DC1}\cdot s + k_{DC2}\cdot s^2\right] F_{Dis}. \tag{28}$$

Inserting (28) in (27), the condition becomes

$$0 \overset{!}{=} \underbrace{F_{Dis}}_{\neq 0}\underbrace{[G_b(s)\cdot G_{DC}(s) + G_e(s)]}_{\overset{!}{=}0}. \tag{29}$$

For a dynamic disturbance compensation, the corresponding ansatz coefficients have to be chosen in such a way that the first three coefficients of the numerator polynomial become zero. The required time derivatives of the disturbance F_{Dis} are calculated by real differentiation.

4. Gain-Scheduled Sliding Mode State Observer

For cost reasons, a sensor for the measurement of the internal pressure p is usually not available in real trucks. As an alternative, an estimation of this state is envisaged. In the following, a gain-scheduled sliding mode state observer is designed according to [3] for the estimation of the internal pressure. Furthermore, it has been shown in [9] that both the pressure and the disturbance force F_U cannot be observed simultaneously in steady-state phases with $\dot{z} = 0$. As a remedy, an effective cylinder pressure – consisting of the sum of the internal pressure and a correction term addressing the contribution of the disturbance force F_U – is introduced with

$$p_e = p + \frac{F_U}{A_K}, \tag{30}$$

which leads to the completely observable system representation

$$\dot{\underline{x}}_o(t) = \underbrace{\begin{bmatrix} 0 & 1 & 0 \\ \dfrac{F_{cl}(z,\dot{z},\xi) - c_{sp} \cdot (z + z_{sp})}{mz} & 0 & -\dfrac{A_k}{m} \\ 0 & \dfrac{n\,p_0}{V(z)} & \dfrac{n\dot{z}}{V(z)} \end{bmatrix}}_{\underline{A}_o = \underline{A}(z,\dot{z})} \underline{x}_o(t) + \underbrace{\begin{bmatrix} 0 \\ 0 \\ \dfrac{n}{V(z)} \end{bmatrix}}_{\underline{b}_o = \underline{b}(z)} u(t), \quad \text{with } \underline{x}_o(t) = \begin{bmatrix} z(t) \\ \dot{z}(t) \\ p_e(t) \end{bmatrix}. \tag{31}$$

In a first step, a transformation matrix $\underline{T}_S$ is calculated to rearrange the state vector in such a way that the unknown states – the effective pressure and the piston velocity – are shifted to the first two positions in the observer state vector

$$\underline{x}_S = \underline{T}_S \underline{x}_o, \quad \text{with } \underline{T}_S = \begin{bmatrix} 0 & 1 & 0 \\ 0 & 0 & 1 \\ \hline \underline{c}_m^T \end{bmatrix} = \begin{bmatrix} 0 & 1 & 0 \\ 0 & 0 & 1 \\ \hline 1 & 0 & 0 \end{bmatrix}. \tag{32}$$

Next, the state dependent system matrices have to be recalculated due to the transformed state vector $\underline{x}_S$

$$\underline{A}_S = \underline{T}_S \underline{A}_o \underline{T}_S^{-1} = \begin{bmatrix} \underline{A}_{11} & \underline{a}_{12} \\ \hline \underline{a}_{21}^T & a_{22} \end{bmatrix} = \begin{bmatrix} 0 & -\dfrac{A_k}{m} & \dfrac{F_{cl}(z,\dot{z},\xi) - c_{sp}\cdot(z+z_{sp})}{mz} \\ \dfrac{n\,p_0}{V(z)} & \dfrac{n\dot{z}}{V(z)} & 0 \\ \hline 1 & 0 & 0 \end{bmatrix}, \tag{33}$$

$$\underline{b}_S = \underline{T}_S \underline{b}_o = \begin{bmatrix} \underline{b}_{S1} \\ \hline b_{S2} \end{bmatrix} = \begin{bmatrix} 0 \\ \dfrac{n}{V(z)} \\ \hline 0 \end{bmatrix} \quad \text{and} \quad \underline{c}_S^T = \underline{c}_m^T \underline{T}_S^{-1}. \tag{34}$$

Then, the sliding mode observer has the form

$$\begin{bmatrix} \dot{\hat{\underline{x}}}_u \\ \dot{\hat{y}} \end{bmatrix} = \begin{bmatrix} \underline{A}_{11} & \underline{a}_{12} \\ \underline{a}_{21}^T & a_{22} \end{bmatrix} \begin{bmatrix} \hat{\underline{x}}_u \\ \hat{y} \end{bmatrix} + \begin{bmatrix} \underline{b}_{S1} \\ b_{S2} \end{bmatrix} u - \begin{bmatrix} \underline{g}_1 \\ g_2 \end{bmatrix} (\hat{y} - y) + \begin{bmatrix} \underline{l} \\ -1 \end{bmatrix} \upsilon, \tag{35}$$

where $\hat{\underline{x}}_u$ contains the unmeasured states $\hat{z}$ and $\hat{p}_e$, and $\hat{y} = \hat{z}$ the measured state. $\underline{g}_1$ and g_2 denote Luenberger type gains, whereas $\underline{l} \in \mathbb{R}^{2 \times 1}$ is a feedback gain vector. The discontinuous input is given by $\upsilon = M_1 \,\text{sgn}(\hat{z} - z)$, with a positive constant gain M_1. Introducing the definitions

$$\underline{e}_1 = \begin{bmatrix} \hat{z} - \dot{z} \\ \hat{p}_e - p_e \end{bmatrix} \tag{36}$$

and $e_y = \hat{z} - z$, (34) and (35) lead to the following dynamics

$$\begin{bmatrix} \dot{\underline{e}}_1 \\ \dot{e}_y \end{bmatrix} = \begin{bmatrix} \underline{A}_{11} & \underline{a}_{12} \\ \underline{a}_{21}^T & a_{22} \end{bmatrix} \begin{bmatrix} \underline{e}_1 \\ e_y \end{bmatrix} - \begin{bmatrix} \underline{g}_1 \\ g_2 \end{bmatrix} e_y + \begin{bmatrix} \underline{l} \\ -1 \end{bmatrix} \upsilon. \tag{37}$$

With a new error variable $\bar{\underline{e}}_1 = \underline{e}_1 + \underline{l}\,e_y$, the error dynamics w.r.t. the state variables $\bar{\underline{e}}_1$ and e_y can be expressed as

$$\begin{bmatrix} \dot{\bar{\underline{e}}}_1 \\ \dot{e}_y \end{bmatrix} = \begin{bmatrix} \underline{A}_{11} + \underline{l}\,\underline{a}_{21}^T & \underline{a}_{12} - (\underline{A}_{11} + \underline{l}\,\underline{a}_{21}^T)\underline{l} - \underline{g}_1 + \underline{l}\cdot(a_{22} - g_2) \\ \hline \underline{a}_{21}^T & a_{22} - g_2 - \underline{a}_{21}^T \underline{l} \end{bmatrix} \begin{bmatrix} \bar{\underline{e}}_1 \\ e_y \end{bmatrix} + \begin{bmatrix} \underline{0} \\ -1 \end{bmatrix} \upsilon. \tag{38}$$

Here, the additional switching input υ affects only the last row. By a proper selection of the gain vector $\underline{g}_1$, the vector

$$\underline{a}_{12} - (\underline{A}_{11} + \underline{l}\,\underline{a}_{21}^T)\underline{l} - \underline{g}_1 + \underline{l}\cdot(a_{22} - g_2) = \underline{0} \tag{39}$$

vanishes. Therefore, in the case of $\upsilon = 0$, the asymptotic stability of the error dynamics (38) can be guaranteed by choosing the gain vector $\underline{l}$ and the scalar gain g_2 as follows

$$\det(s - (\underline{A}_{11} + \underline{l}\,\underline{a}_{21}^T)) \overset{!}{=} (s + p_1)^2, \tag{40}$$

$$\det(s\underline{I} - (a_{22} - g_2 - \underline{a}_{21}^T \underline{l})) \overset{!}{=} (s + p_2), \tag{41}$$

where $p_1 > 0$ and $p_2 > 0$ determine the desired characteristic polynomials of the block diagonal matrices, respectively. The additional switching input υ yields the potential to provide robustness against certain classes of model uncertainty. Considering chattering that may be caused by the discontinuous components, the tanh function is used in the implementation instead of the sgn function.
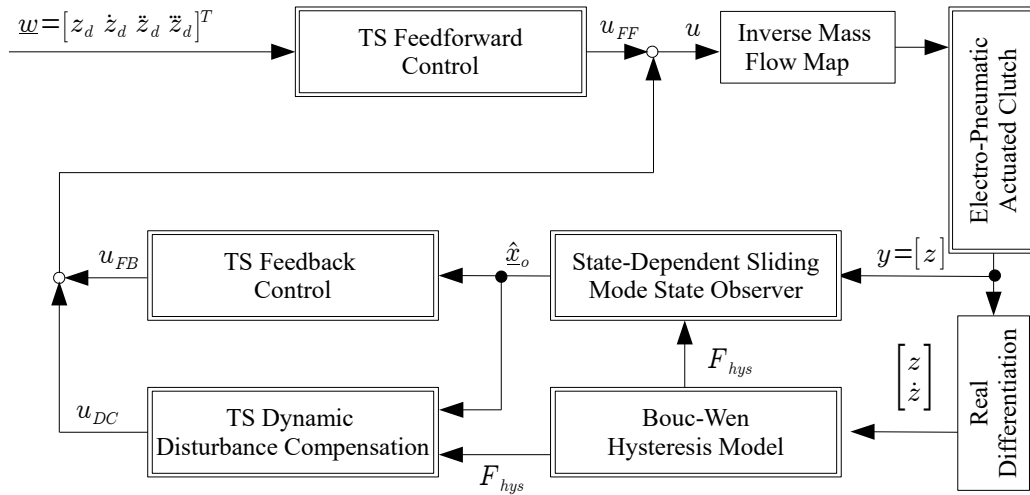
5. Experimental Results

Figure 6: Block diagram of the implemented control structure.

The overall control structure – involving feedback control, feedforward control, and observer-based disturbance estimation as well as disturbance compensation – is shown in Fig. 6. Note that a hysteresis model is employed for a correction of both the state observer and the disturbance compensation, evaluated with measured values. The pneumatic valve characteristics are compensated by inverse flow maps. A dSPACE real-time system is used to drive the test rig. The supply pressure p_S for the on-off-valves is available at a level of $p_S \approx 9 \cdot 10^5$ Pa. The desired trajectory for the clutch position as well as its corresponding time derivative are depicted in Fig. 7. The clutch is fully closed at $z = z_{zu} = 0.0385$ m. Furthermore, different scenarios are presented in the desired trajectory: a complete opening and closing of the clutch for e.g. gear shifting is considered as well as a simulated step-wise start-up of the truck.

(a) Desired trajectory for the position of the clutch.

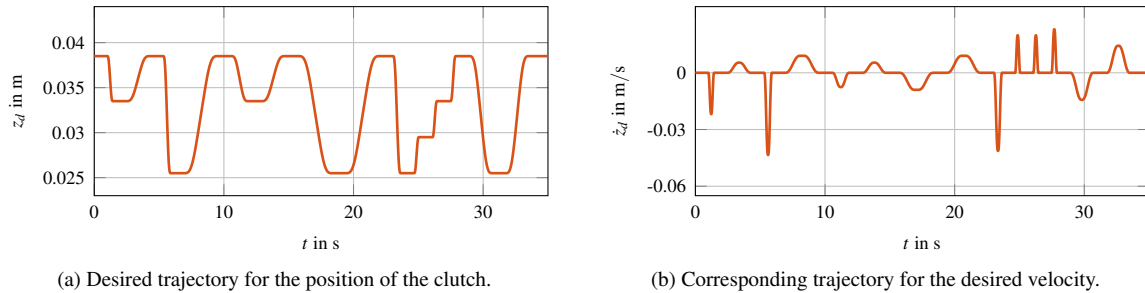(b) Corresponding trajectory for the desired velocity.

Figure 7: Desired values for the experimental investigation of the clutch.

The overall control concept has been successfully validated at a test rig at the Chair of Mechatronics, University of Rostock. The corresponding experimental results for the tracking behaviour with small tracking errors are presented in Fig. 8. The maximum absolute position error is $\max(|e|) \approx 2$ mm, which occurs at $t \approx 28$ s. For the purpose of a parameter identification, a pressure sensor is installed at the test rig. As already mentioned in Sect. 4, however, a pressure sensor is not available in real trucks. Therefore, an estimation of the effective pressure is performed by a sliding mode state and disturbance observer. The obtained results are depicted in Fig. 9, which indicate an accurate estimation of the internal chamber pressure.

6. Conclusions

In this paper, a model-based control concept for a electro-pneumatic clutch is presented. First, a control-oriented model is derived based on physical modelling. Thereby, the main nonlinearities can be attributed to the clutch force characteristics with hysteresis and to the pneumatical subsystem. The control design is based on an exact Takagi-Sugeno representation, where the nonlinear control-oriented model is written in a quasi-linear form. Considering the given bounds of the nonlinear terms, four corner models with constant system matrices and corresponding membership functions are introduced. In each corner, a linear state feedback is designed. With the help of a pseudo inverse, a norm-optimal adaptive feedback gain vector can be derived that leads to a constant closed-loop system matrix. The specified eigenvalues guarantee, hence, asymptotical stability of the controlled system. Furthermore, a model-based feedforward control and a dynamic disturbance compensation are designed to improve the tracking behaviour regarding a desired trajectory for the clutch

(a) Desired and measured position of the clutch.
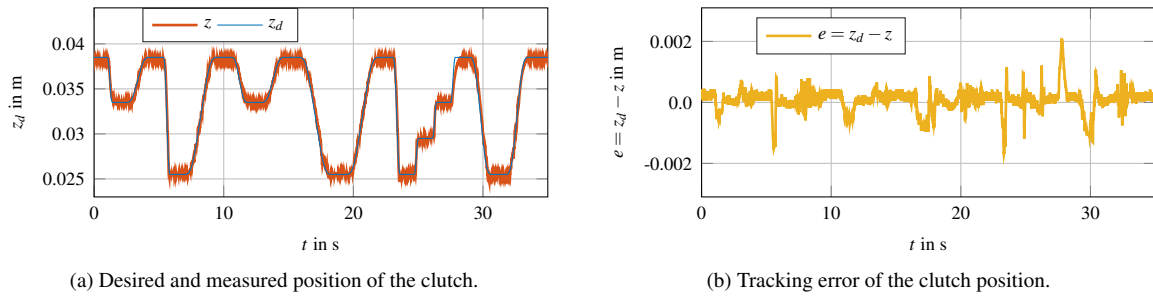

(b) Tracking error of the clutch position.

Figure 8: Comparison of desired and measured values (a) and the corresponding tracking error (b) regarding the clutch position (experimental results).
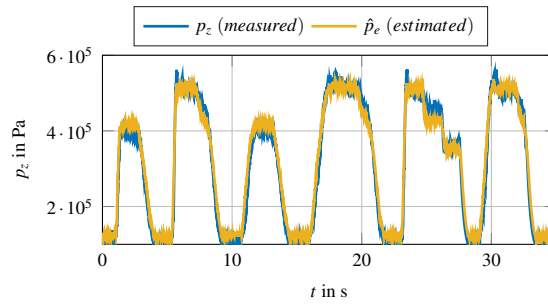

Figure 9: Measured internal pressure and estimated effective pressure (experimental results).

position. Additionally, a sliding mode state observer is designed to estimate an effective pressure in the chamber. Finally, the overall control structure has been successfully validated on a dedicated test rig available at the Chair of Mechatronics, University of Rostock.

References

[1] Aschemann, H., Prabel, R., and Schindele, D.: Hysteresis Compensation and Adaptive LQR Design for an Electropneumatic Clutch for Heavy Trucks. In *European Control Conference (ECC)*, 2013, pp. 1475–1480.

[2] Aschemann, H., Schindele, D., and Prabel, R.: Observer-Based Control of an Electro-Pneumatic Clutch Using Extended Linearisation Techniques. In *17th International Conference on Methods and Models in Automation and Robotics (MMAR)*, 2012, pp. 493–498.

[3] Edwards, C. and Spurgeon, S.: Sliding Mode Control: Theory And Applications. In *Series in Systems and Control* Taylor & Francis, 1998.

[4] Georg, S. and Schulte, H.: Actuator Fault Diagnosis and Fault-Tolerant Control of Wind Turbines Using a Takagi-Sugeno Sliding Mode Observer. In *Intl. Conf. on Control and Fault-Tolerant Systems (SysTol)*, 2013, pp. 516–522.

[5] Gonzalez, T., Rivera, T. and Bernal, M.: Nonlinear Control for Plants with Partial Information via Takagi-Sugeno Models: An Application on the Twin Rotor MIMO System. In *9th Intl. Conf. on Electrical Engineering, Computing Science and Automatic Control (CCE)*, 2012, pp. 1–6.

[6] Langjord, H., Kaasa, G.O., and Johansen, T.A.: Nonlinear Observer and Parameter Estimation for Electropneumatic Clutch Actuator. In *IFAC Symposium on Nonlinear Control Systems*, 8, 2013, pp. 789–794.

[7] Pica, G., Cervone, C., Senatore, A., Lupo, M. and Vasca, F.: Dry Dual Clutch Torque Model with Temperature and Slip Speed Effects. In *Intelligent Industrial Systems*, 2016, vol. 2, num. 2, pp. 133–147.

[8] Pisaturo, M., Senatore, A. and D'Agostino, V.: Automotive Dry-Clutch Control: Engagement Tracking and FE Thermal Model. In *IEEE 20th Jubilee International Conference on Intelligent Engineering Systems (INES)*, 2016, pp. 69–74.

[9] Prabel, R. and Aschemann, H.: State-Dependent Sliding Mode Observer for an Electro-Pneumatic Clutch. In *Intl. Conf. on Advanced Intelligent Mechatronics (AIM)*, 2016.

[10] Tanaka, K. and Wang, H.O.: Fuzzy Control Systems Design and Analysis: A Linear Matrix Inequality Approach, Wiley, 2001.

[11] Vasca, F., Iannelli, L., Senatore, A. and Reale, G.: Torque Transmissibility Assessment for Automotive Dry-Clutch Engagement. In *IEEE/ASME Transactions on Mechatronics*, 2011, vol. 16, num. 3, pp. 564–573.